JMEPEG (2018) 27:1369–1377
https://doi.org/10.1007/s11665-018-3224-y

1059-9495/$19.00

Surface Texturing of Polyimide Composite by Micro-Ultrasonic Machining

N.S. Qu, T. Zhang, and X.L. Chen

(Submitted January 21, 2017; in revised form January 10, 2018; published online February 16, 2018)

In this study, micro-dimples were prepared on a polyimide composite surface to obtain the dual benefits of polymer materials and surface texture. Micro-ultrasonic machining is employed for the first time for micro-dimple fabrication on polyimide composite surfaces. Surface textures of simple patterns were fabricated successfully with dimple depths of 150 μm, side lengths of 225-425 μm, and area ratios of 10-30%. The friction coefficient of the micro-dimple surfaces with side lengths of 325 or 425 μm could be increased by up to 100% of that of non-textured surfaces, alongside a significant enhancement of wear resistance. The results show that surface texturing of polyimide composite can be applied successfully to increase the friction coefficient and reduce wear, thereby contributing to a large output torque.

Keywords friction, micro-dimple, micro-ultrasonic machining, surface texture, ultrasonic motor

1. Introduction

Ultrasonic motors featuring small size, low weight, compact structure, fast response times, low noise, and no electromagnetic interference have been widely used in equipment designed for precise and accurate speed and positioning (Ref 1-3). Ultrasonic motors generate mechanical movement and torque through frictional contact forces between the stator and rotor or slider by utilizing the vibration of the elastic stator in the ultrasonic frequency band and the reverse piezoelectric effect of piezoelectric materials (Ref 1). Because the mechanical vibrations are converted to linear or rotary motion by frictional forces generated in the stator–rotor interface, both the efficiency of energy conversion and the operating life of ultrasonic motors depend to a great extent on the properties of frictional forces. The friction coefficient of the sliding surface therefore plays an important role in the output characteristics and life span of ultrasonic motors, and an appropriate level of friction coefficient—varying according to motor type and driving conditions—is essential for ultrasonic motors. In ultrasonic motors, the contact interfaces need to possess both high friction coefficients and excellent wear resistance. In some previous reports on ultrasonic motors, polymer films, including polyimide (PI) composite, polytetrafluoroethylene (PTFE) composite, polyvinylidene fluoride (PVDF), polyetheretherketone (PEEK), and polyphenylenesulfide (PPS), were glued to the contacting surface to improve the friction coefficients and wear characteristics (Ref 4-6).

Recently, the application of surface textures, including micro-dimples, micro-pillar, and micro-grooves, has been employed to improve the tribological performance of various engineering components (Ref 7-9). The results of these studies indicated that the different geometrical properties of micro-dimple surfaces, such as shape, diameter, depth, and area ratio, have a significant influence on tribological performance (Ref 10). Under dry and oil-lubricated conditions, surface textures with different parameters were able to not only reduce friction coefficients but also increase them (Ref 10, 11). For ultrasonic motors, enhancement of the friction coefficient is beneficial for obtaining a high output torque in dry friction conditions. The present paper focuses on the enhancement of the friction coefficient in the contact interface of ultrasonic motors.

To generate surface textures, several micro-texturing techniques can be employed, such as laser texturing (LST), electrical discharge machining (EDM), electrochemical machining (ECM), and micro-ultrasonic machining (MUSM) (Ref 12, 13). Non-conducting non-metallic materials cannot be machined by ECM or EDM. Compared with other methods, MUSM is a promising machining technique with the following advantages: It is independent of material conductivity, it is capable of machining all kinds of hard and brittle materials, it requires a relatively small cutting force and cutting heat, it does not introduce deformation or burn, and it is convenient for machining a variety of complex structures (Ref 14-16). Dimple arrays with a diameter of 300 μm and depth of 600 μm were successfully generated by PZT USM (Ref 17). Reference 18 developed an ultrasonic elliptical vibration texturing system and fabricated micro-groove textures to reduce the adhesion of the rake face of carbide cutting tools. So far, MUSM has mostly been applied to process hard and brittle materials, such as ceramic, silicon, and glass, because polymers are usually too soft to be machined by USM. However, among new kinds of polymers being developed, some products with good mechanical properties have been found. For example, polyimide composite is a kind of polymer material containing various additives that enhance its mechanical properties. However, it has not been reported whether USM might be used to treat this material.

In this paper, surface texturing of polyimide composite by MUSM is described for the first time. The influence of variations in abrasive particle size, abrasive concentration, and static load on the size of dimples is investigated. A dry friction

N.S. Qu, T. Zhang, and **X.L. Chen**, College of Mechanical and Electrical Engineering, Nanjing University of Aeronautics and Astronautics, Nanjing 210016, China. Contact e-mail: nsqu@nuaa.edu.cn.

test is also performed on the friction pair to investigate the influence of textured polyimide composite on the friction coefficient and wear characteristics.

2. Materials and Methods

MUSM accomplishes the removal of material by the abrasive action of a particle-loaded slurry between the workpiece and a tool that is vibrated at low amplitude (related to the power rating) and high frequency (usually 16-25 kHz). For this paper, experiments were conducted in a precise, integrated USM machine system (Fig. 1) (BDC-150F; Beijing DMBEST Tool and Die Tech Co., Ltd), consisting of an ultrasonic generator, ultrasonic transducer, ultrasonic horn, tool, working stage, power supply, and control unit. A high-power amplifier IC was used in the ultrasonic generator, and the ultrasonic vibration was generated by a digital piezoelectric transducer. It has the function of automatic frequency tracking and can maintain system resonance by automatic controls. The input power ranges from zero to 150 W with a frequency of 20 ± 4 kHz (the resonance frequency of the vibrator). The workpiece was fixed on the stage, and the abrasive was refreshed manually because of the small machining area and depth.

The workpiece material investigated in this study was polyimide composite, whose major properties at room temperature are listed in Table 1. The ultrasonic tool with a micro-square cylinder array (Fig. 2) was fabricated by wire-EDM using mild steel.

The selected range of parameters listed in Table 2 was based on the results of pilot experiments during machining of square micro-dimple arrays on polyimide composite samples. Boron carbide was employed as the abrasive material in this research because of its economy and cutting rate.

The slurry was prepared in four different concentrations: 5, 15, 30, and 45% (wt% of abrasive in water). The static load applied varied from 1.5 to 10 N, and all experiments were performed with a machining time of 15 s. The performance of the aforementioned process parameters on the size of dimples machined was evaluated by determining the influence of each parameter, while all others remained constant.

Aluminum is a popular material used for the rotor of ultrasonic motors, and tin bronze is employed as the stator. To

Table 1 Properties of polyimide composite

Property	Value
Roughness, Ra	350 nm
Density	1.4 g cm^{-3}
Tensile strength	130 MPa
Breaking elongation	7%
Flexural strength	131 MPa
Flexural modulus	3.35 GPa
Compression modulus	1.5
Ball indentation hardness	169 MPa

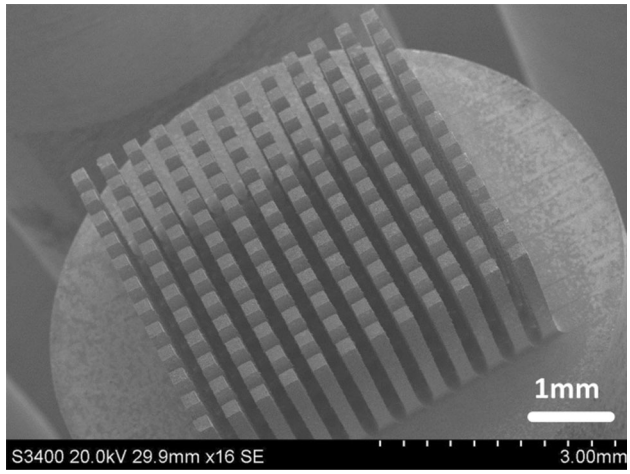

Fig. 2 Scanning electron microscope (SEM) image of ultrasonic tool with micro-square cylinder array (side length 200 μm, height 2 mm, area ratio 30%)

Table 2 Parameter settings employed in experiments

Parameter	Value
Abrasive particle size	1 μm, 10 μm, 40 μm
Abrasive concentration	5%, 15%, 30%, 45%
Static load	1.5 N, 3 N, 5 N, 7 N, 20 N

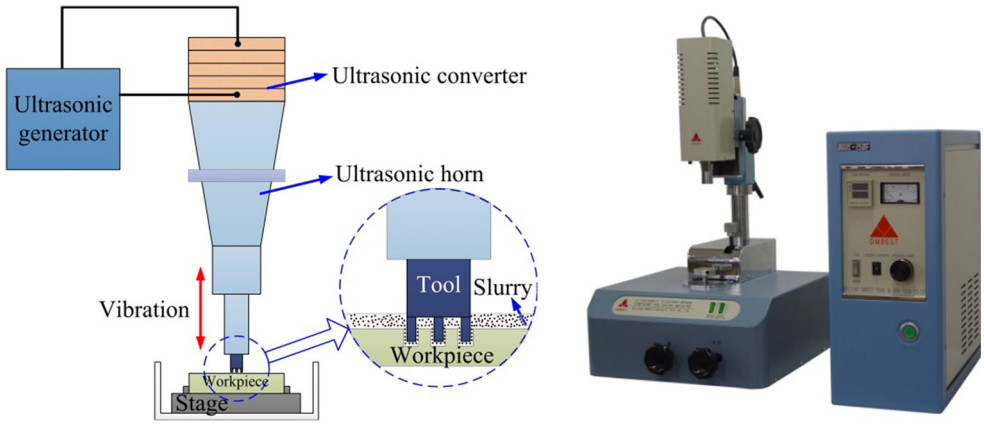

Fig. 1 Schematic diagram and picture of MUSM machining system

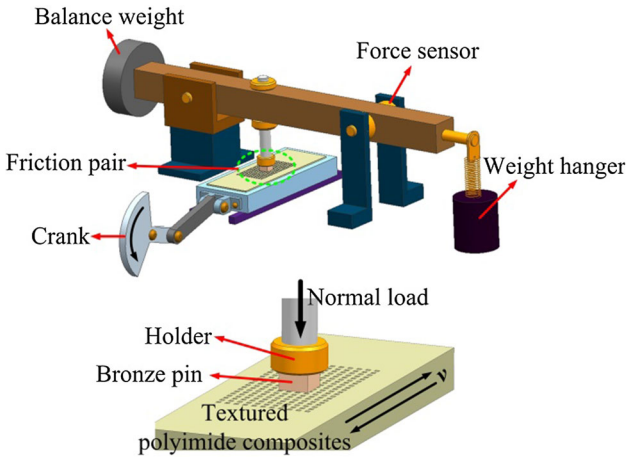

Fig. 3 Schematic diagram of the sliding friction test

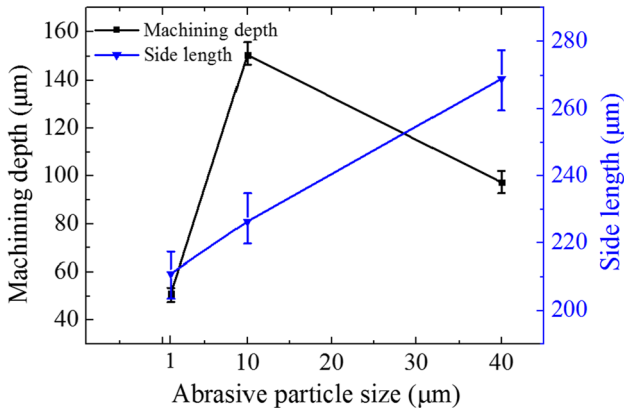

Fig. 4 Effect of abrasive particle size on the machining depth and side length of micro-dimples (concentration 15%, static load 7 N, power rating 135 W)

increase the friction coefficient as well as reduce the wear between the rotor and stator, the textured polyimide composite material is laminated onto the rotor. Friction tests were performed using a pin-on-flat tribometer under dry friction conditions (Fig. 3). The lower samples were polyimide composite blocks driven by a crank system under linear reciprocating motion at a constant frequency. The upper specimens were tin bronze pins fixed into a metallic holder. Both the friction coefficient and wear were investigated.

Before the tests began, all of the samples were cleaned ultrasonically in an acetone bath for 3 min. The tests were conducted at a normal load of 60 N, a frequency of 5 Hz, and a stroke length of 1.5 mm in a laboratory atmosphere (25 °C, relative humidity 55%). The side length of the tin bronze was 2.5 mm, giving an apparent contact pressure in all the tests of 9.6 MPa. It took 10 min to complete the running-in process for all of the specimens. The friction coefficient was obtained by averaging the data over the following 20 min.

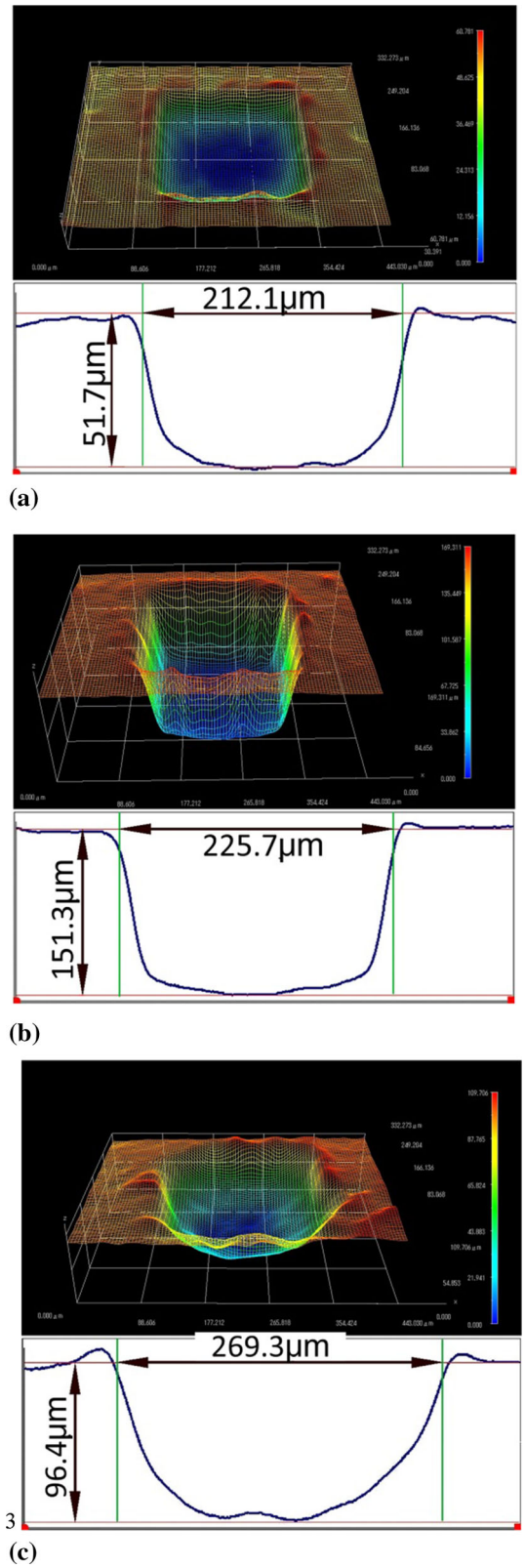

Fig. 5 Micro-dimple profiles fabricated with different abrasive particle sizes

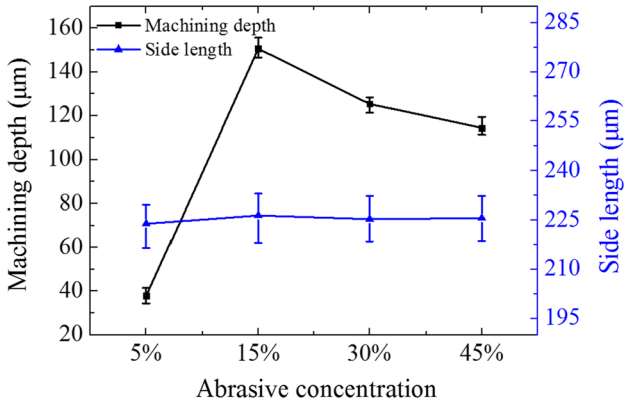

Fig. 6 Effect of abrasive concentration on the machining depth and side length of micro-dimples (static load 7 N, abrasive particle size 10 μm, power rating 135 W)

3. Results and Discussion

3.1 Effect of Abrasive Particle Size

The effect of abrasive particle size on the micro-dimples is shown in Fig. 4 at an abrasive concentration of 15%, a static load of 7 N, and a power rating of 135 W. The machining depth and side length were 51.0 μm and 211 μm, respectively, for an abrasive particle size of 1 μm. When the abrasive particle size was increased to 10 μm, the machining depth and side length increased to 150 and 226 μm, respectively. However, when the abrasive particle size was increased further to 40 μm, the machining depth reduced to 97 μm and the side length increased to 269 μm. This suggests that a small machining depth is obtained when a larger abrasive particle size is selected. This result can be explained by the fact that as the abrasive particle size was increased, the amplitude of the tool vibration could not provide sufficient space between the tool face and the workpiece; thus, little cavitation erosion occurred. In addition, the quantity of abrasive particles decreased when the size of the abrasive particles was increased at the same slurry concentration. A smaller abrasive particle size also led to a small machining depth because of the low kinetic energy of a single abrasive particle. As a result, the size of the dimples machined increased with the increase in abrasive particle size. Figure 5(a), (b), and (c) shows the profiles of micro-dimples fabricated with abrasive particles of the three aforementioned sizes. It can be seen that micro-dimples with large, rounded corners formed with large abrasive particle size. In addition, a convex shape appeared in the center of the micro-dimple formed in the case with large abrasive particle size. This can be explained by an increase in abrasive particle size making it difficult for the abrasive particles to flow into the machining area, which results in the area with the lowest number of abrasive particles being in the center of the micro-dimple—hence the convex shape appearing. Moreover, the uniformity of the abrasive particles' distribution was poor, which led to a non-smooth surface machined at the bottom of the micro-dimple.

3.2 Effect of Abrasive Concentration

Figure 6 and 7 show the effect of abrasive concentration on the micro-dimples, while other parameters were kept constant,

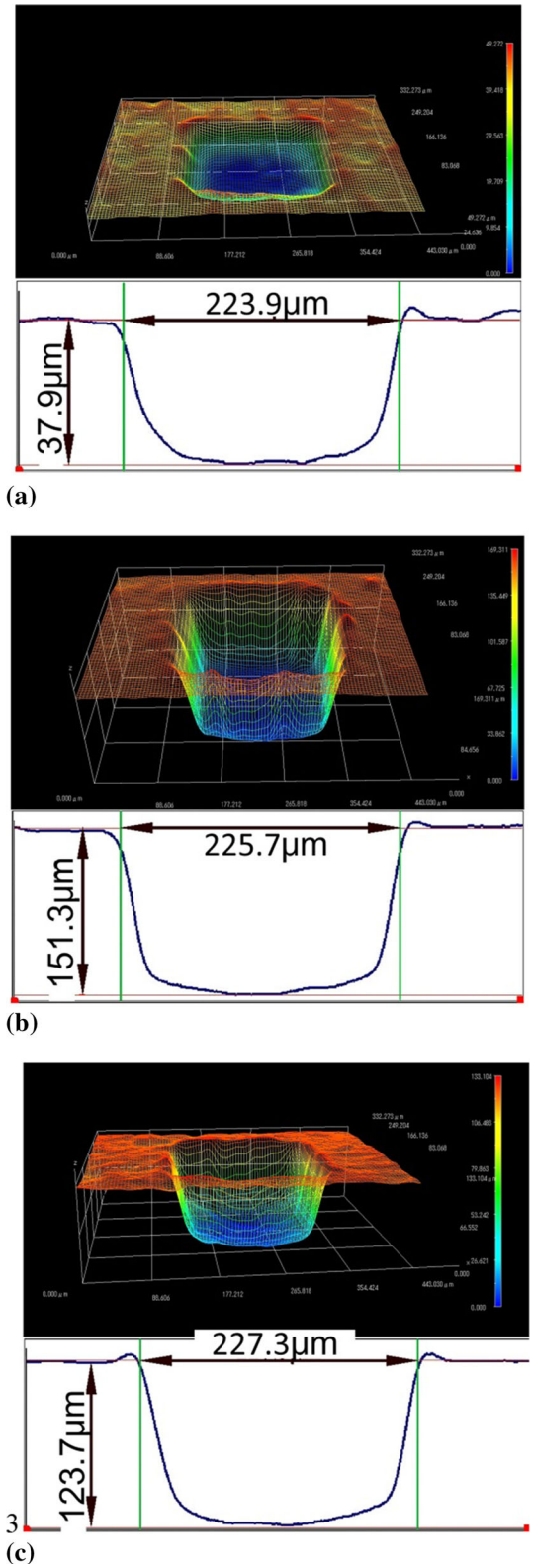

Fig. 7 Micro-dimple profiles fabricated with different abrasive concentrations

i.e., an abrasive particle size of 10 μm, a static load of 7 N, and a power rating of 135 W. It can be seen that the side length of the machined micro-dimples was scarcely affected by a change in the abrasive concentration. The machining depth and side

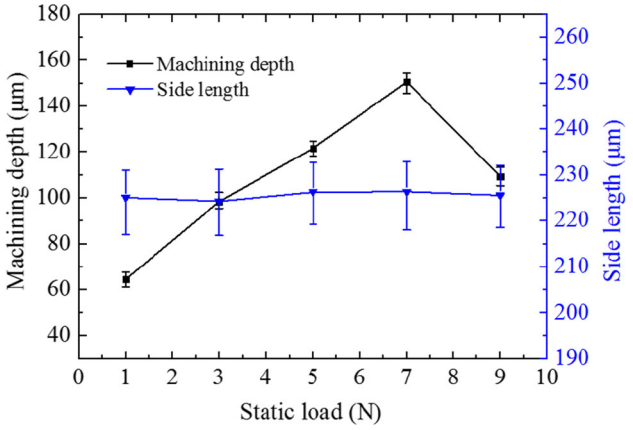

Fig. 8 Effect of static load on the machining depth and side length of micro-dimples (concentration 15%, abrasive particle size 10 μm, power rating 135 W)

length were 38 and 224 μm, respectively, at 5% abrasive concentration. When the abrasive concentration was increased to 15%, the machining depth increased to 151 μm with almost no change in the side length. However, when the abrasive concentration was increased further, the machining depth actually decreased, and the same phenomenon occurred for the side length. It can be seen that the greatest machining depth was obtained with an abrasive concentration of 15%. A low abrasive concentration means that there are few abrasive particles in the machining gap, so less erosion of material occurs, leading to a small machining depth. The machining depth increases with abrasive concentration because there are more active abrasive particles available in the gap between the tool and the workpiece. However, a decreased machining depth is obtained with a high abrasive concentration because both the circulation and impact of the abrasive particles on the workpiece in the machining area are affected, with a corresponding negative effect on machining depth.

3.3 Effect of Static Load

In MUSM, an adaptive feed is implemented by means of springs or by magnetic, hydraulic, or gravitational forces instead of the tool being fed rigidly at a constant speed. Static load is therefore an important parameter in MUSM. The effect of static load on the micro-dimples is shown in Fig. 8 and 9 for a 10-μm abrasive particle size, 15% abrasive concentration, and 135-W power rating. An appropriate static load between the tool and workpiece should be ensured. The static load has a remarkable effect on machining depth but little effect on the side length of the micro-dimples. A light static load leads to poor machining depth because the increase in the gap between the tool face and the workpiece weakens the impact and depth of the abrasive on the workpiece. During the impact process, there is too much energy loss, and hence the impact is weakened. Too large a static load may similarly not contribute to machining depth because the decrease in the gap between the tool face and the workpiece blocks the abrasive particles from entering the machining area and removing the product. Higher loads decrease the amplitude of tool tip vibration and prolong the contact time. Excessive loads can lead to improper vibration

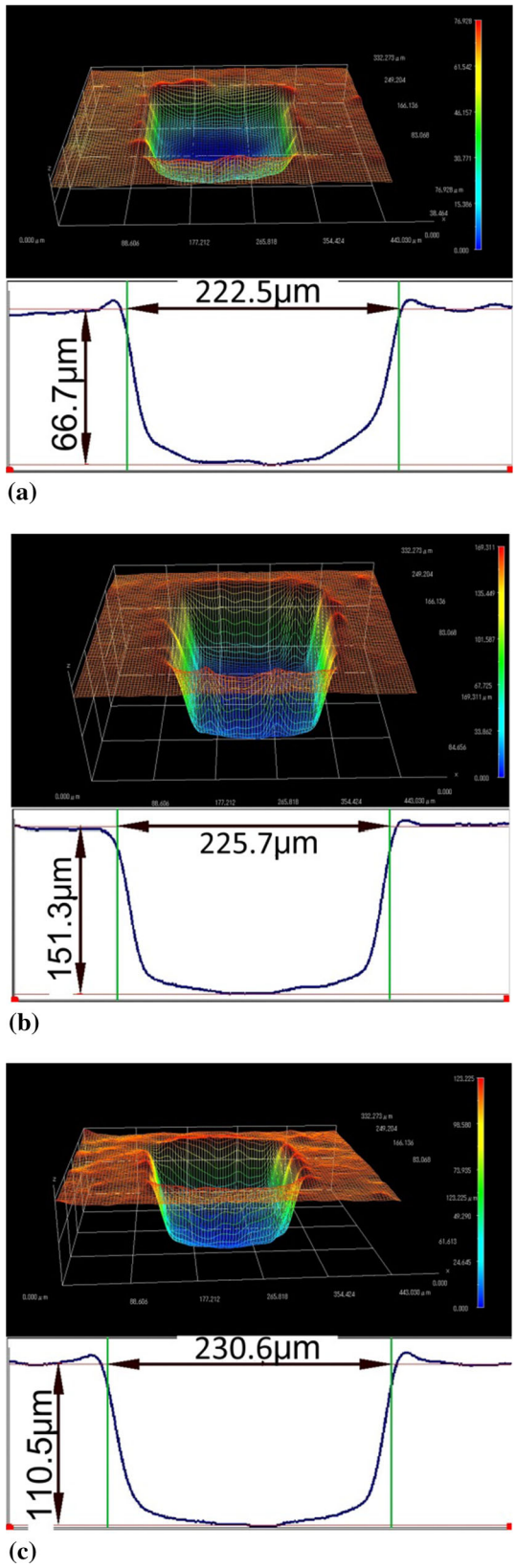

Fig. 9 Micro-dimple profiles fabricated with different static loads

of the tool and are also not beneficial for improving machining depth. The side length of the micro-dimples machined was largely unaffected by the static load.

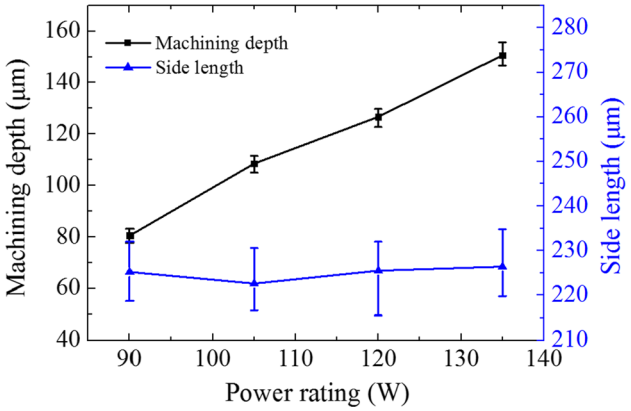

Fig. 10 Effect of power rating on the machining depth and side length of micro-dimples (concentration 15%, abrasive particle size 10 μm, static load 7 N)

3.4 Effect of Power Rating

The effect of power rating on the micro-dimples is shown in Fig. 10 and 11 for a 10-μm abrasive particle size, 15% abrasive concentration, and a static load of 7 N. It can be seen that the machining depth increased with the power rating, with the biggest machining depth obtained when the highest power rating of 135 W was applied. The amplitude of the tool tip vibration increased with the power rating. A large amplitude leads to a large dynamic force on the workpiece, which means an increase in the momentum and kinetic energy of the abrasive particles in slurry hammering. Moreover, a large amplitude of the tool tip vibration is also beneficial for flushing away the machining products. Both of these positive effects should lead to an increased machining depth. It is important to note that the side length of micro-dimples machined was largely unaffected by the power rating.

3.5 Tribological Evaluation of Textured Surfaces

To assess the effect of the micro-dimple arrays on the tribological properties of polyimide composite, the friction coefficients of the surfaces with and without micro-dimple arrays were investigated under a load of 60 N. Tools with a micro-square cylinder array of different sizes (Table 3) were fabricated (Fig. 12).

Micro-dimple arrays of various dimensions were pattern machined onto the sample surface using MUSM (abrasive particle size 10 μm, abrasive concentration 15%, static load 7 N, power rating 135 W). Figure 13 shows the micro-dimple arrays generated with side lengths of 225 ± 5, 325 ± 5, and 425 ± 5 μm at a depth of 150 ± 5 μm and an area ratio of approximately 30%.

The test results from these samples are shown in Fig. 14. Compared with a non-dimple surface, the samples with micro-dimple arrays had increased friction coefficients. The pattern with a dimple side length of 225 μm did not lead to a significant increase in the friction coefficient, but applying a pattern with dimple side lengths of 325 or 425 μm increased the friction coefficient to as high as 0.3, which is nearly twice that of the non-dimple pattern and shows an effective way to increase the friction coefficient. By comparing the friction coefficient of samples with the same side length and different area ratios, it was found that for a dimple side length of

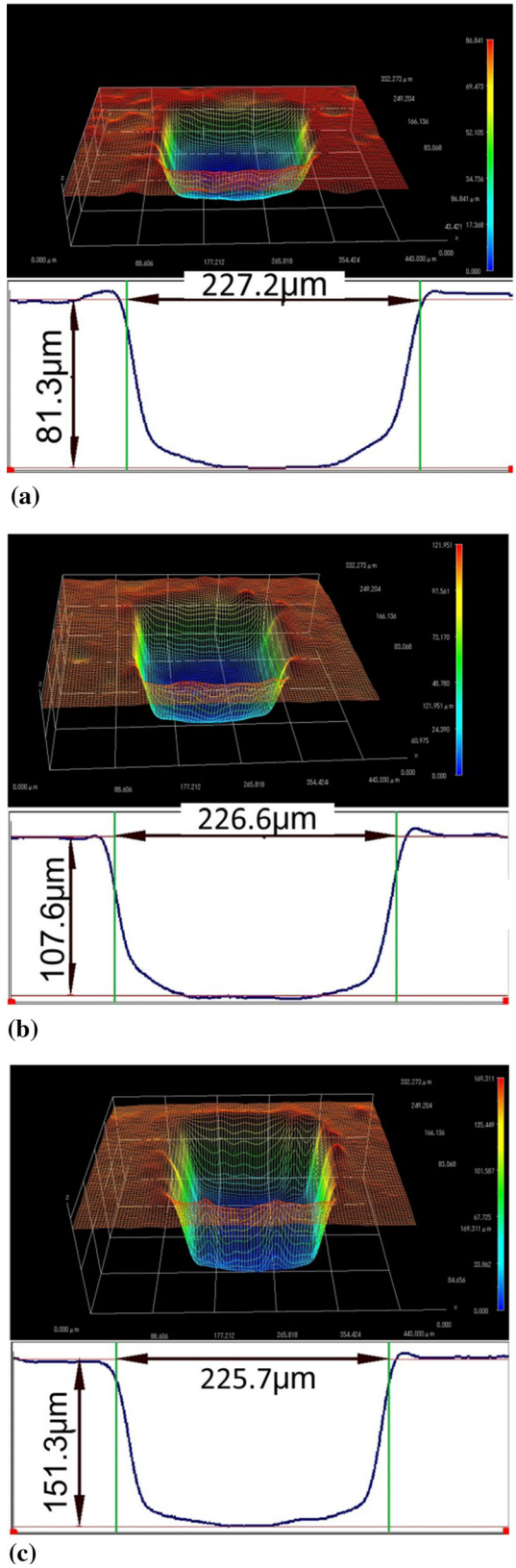

Fig. 11 Micro-dimple profiles fabricated with different power ratings

325 μm, the friction coefficient increased with the area ratio, increasing to approximately 0.35 for an area ratio of 30%. For a dimple side length of 425 μm, a maximum friction coefficient

Table 3 Size of tools employed with micro-square cylinder array

Height	Side length, μm	Area ratio, %
2 mm	200 300 400	10, 20, 30

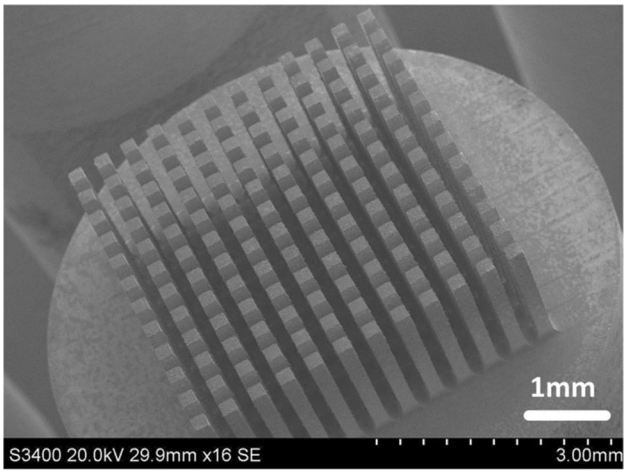

(a)

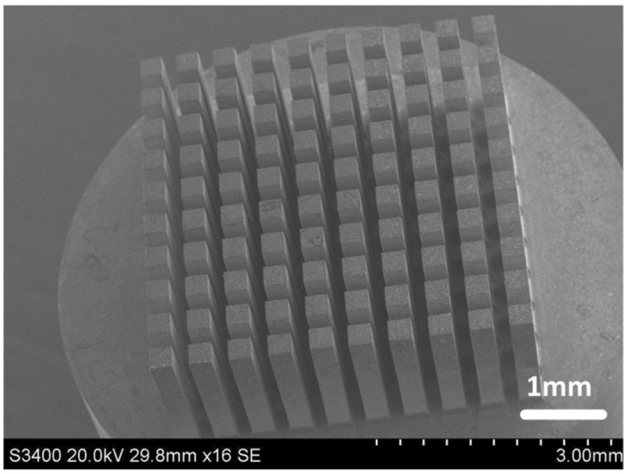

(b)

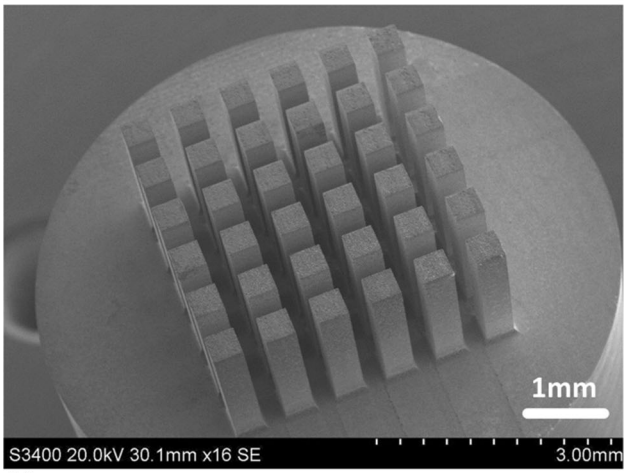

(c)

Fig. 12 SEM images of ultrasonic tool with micro-square cylinder arrays of different side lengths (area ratio 30%)

of 0.326 was observed for an area ratio of 20%. These results indicate that the maximum friction coefficient could be obtained for conditions of dimple side length equal to 325 μm and an area ratio of 30%.

It is well known that the friction coefficient is associated with adhesion, plowing, and deformation and collision of asperities (Ref 11). Compared with the non-dimple surface, the

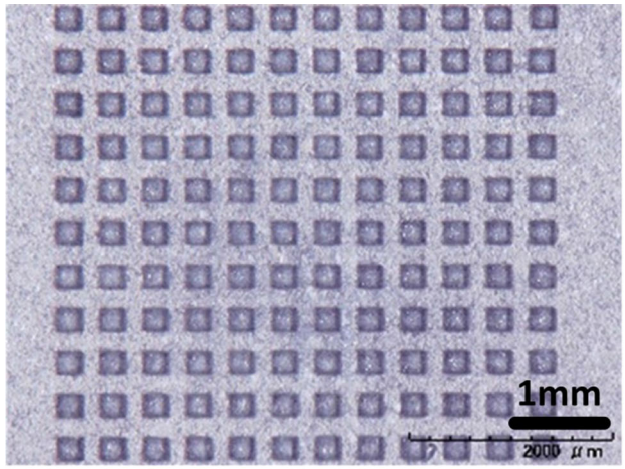

(a)

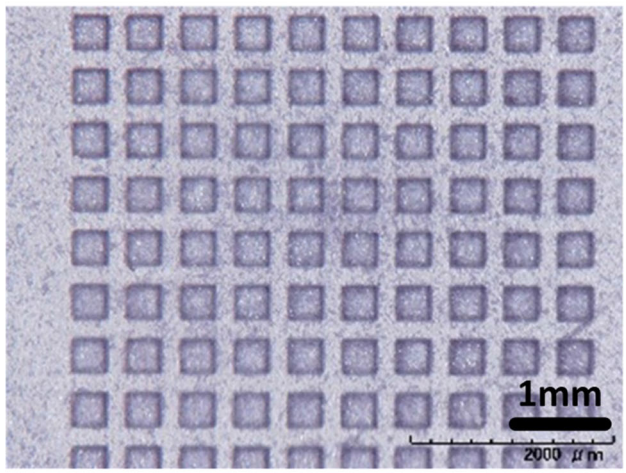

(b)

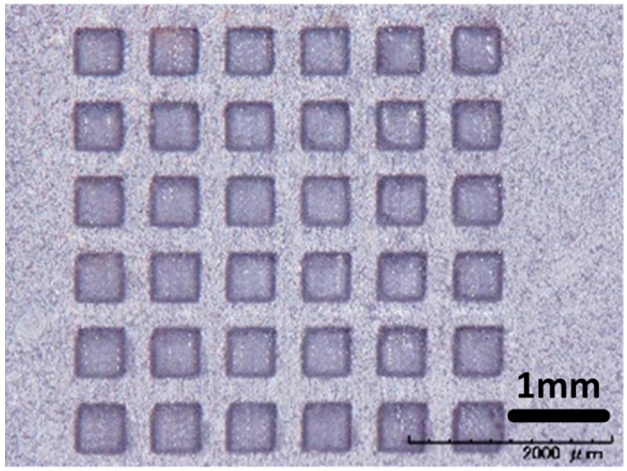

(c)

Fig. 13 Micro-dimple arrays machined by MUSM

real contact area between two micro-dimple surfaces sliding relative to each other reduces, which results in weak adhesion and plowing. Plowing is weakened further because the wear particles can be trapped by the micro-dimples. All of this reduces the friction coefficient. However, compared with non-dimple surfaces, larger deformations of asperity components occur in micro-dimple surfaces, which would increase the friction coefficient. A change in the friction coefficient is considered to be related to these three competing factors. For the micro-dimple surface of 225 μm side length and 10% dimple area ratio, it is known that the effect of deformation of the asperity component is almost the same as that of adhesion and plowing. Therefore, compared with the non-dimple surface, little change in the friction coefficient occurs with this dimple surface. Moreover, with increasing micro-dimple area ratio, the real contact area between two surfaces sliding relative to each other increases, which leads to the enhancement of adhesion and plowing and to weakness in deformation, which results in a gradual increase in the friction coefficient. For the micro-dimple surface with 325 μm side length and 10% dimple area density, the effect of deformation of the asperity component is greater than with that of adhesion and plowing, leading to a rapid increase in the friction coefficient. A similar phenomenon is also observed in a micro-dimple surface of 425 μm side length. Compared with the micro-dimple surface of 225 μm side length, a greater deformation occurred for side lengths of 325 and 425 μm, which resulted in a prompt increase in the friction coefficient. Reference 19 reported that the enhancement in friction between polydimethylsiloxane (PDMS) and a rabbit small-intestinal tract might be obtained by altering the size and pillar density of micro-pillar surfaces. In short, the friction coefficient of micro-dimple surfaces of polyimide composite can be tailored by altering their size and dimple density, which is significant for USM.

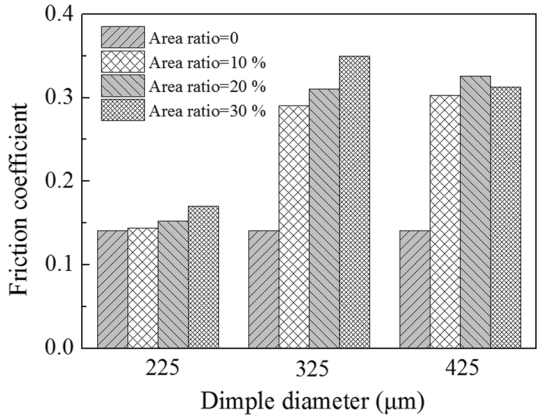

Fig. 14 Effect of micro-dimple arrays on the friction coefficient

Figure 15 shows the morphology of the wear track on both flat and micro-dimple surfaces. The wear resistance of the flat surface is obviously lower than that of the micro-dimple

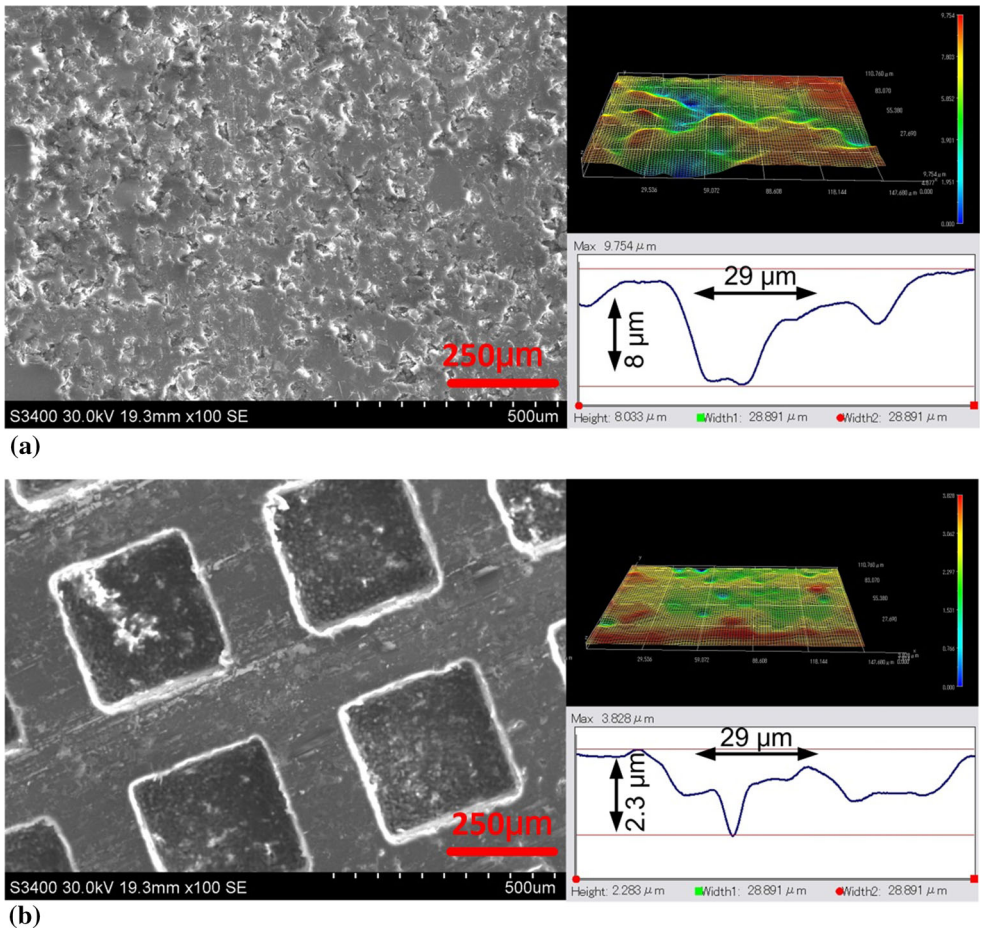

Fig. 15 SEM images of (a) flat and (b) dimpled surface after friction test

surface. Abrasive and adhesive wear occurred simultaneously on the flat surface. Reference 20 reported similar results in their experimental investigation of the tribological behavior of several polymer materials. However, abrasive wear was not observed on the micro-dimple surface. This is because the wear particles can be trapped by the micro-dimples, reducing the frictional plowing component. Therefore, surface texturing of polyimide composite is beneficial for increasing the friction coefficient and for reducing wear, which is helpful for obtaining a large output torque.

4. Conclusions

In this paper, MUSM was used for the first time for micro-dimple fabrication on polyimide composite surfaces. In MUSM, the side length of micro-dimples increases with the abrasive particle size; abrasive concentration and static load have little effect on it. However, the machining depth of micro-dimples increases with the abrasive particle size, abrasive concentration, and initial static load. Simple patterns of surface textures with dimple depths of 150 μm, side lengths of 225-425 μm, and area ratios of 10-30% were fabricated. It was demonstrated clearly that surface texture could increase friction under a load of 60 N. The friction coefficient of the micro-dimple surface with a side length of 325 or 425 μm could be increased by up to 100% of that of non-textured samples, and its wear resistance was significantly enhanced at the same time. The results show that surface texturing of polyimide composite has the dual beneficial effects of increasing the friction coefficient and reducing wear—useful for obtaining a large output torque.

Acknowledgments

The work described in this study was supported by the National Basic Research Program of China (973 Program, Grant 2015CB057502).

References

1. C.S. Zhao, *Ultrasonic Motor: Technologies and Applications*, Science Press, Beijing, 2010, p 1–149
2. W. Qiu, Y. Mizuno, M. Tabaru, and K. Nakamura, Can Lubricant Enhance the Torque of Ultrasonic Motors? An Experimental Investigation, *Appl. Phys. Lett.*, 2014, **105**, p 224102
3. T. Mashimo, Micro Ultrasonic Motor Using a Cube with a Side Length of 0.5 mm, *IEEE ASME Trans. Mech.*, 2016, **21**, p 1189–1192
4. Y.Y. Qu, Y.H. Zhang, and J.J. Qu, Micro-Driving Behavior of Carbon-Fiber-Reinforced Epoxy Resin for Standing-Wave Ultrasonic Motor, *Polym. Compos.*, 2016, **37**, p 2152–2159
5. Q.J. Ding, G. Zhao, H.M. Peng, Y.D. Zhang, and H.F. Li, Properties of Carbon Fiber Reinforced Poly (Vinylidene Fluoride)-Based Friction Materials of Ultrasonic Motors, *Polym. Compos.*, 2016, **37**, p 547–552
6. R.M. Tieck, G.P. Carman, and A. Novel Approach, A Novel Approach to Improving the Available Power Output of Piezoelectric Ultrasonic Motors, 2004 IMECE, Nov 13–20 (California), *Am. Soc. Mech. Eng.*, 2004, **2004**, p 941–948
7. P.G. Grutzmacher, A. Rosenkranz, and C. Gachot, How to Guide Lubricants: Tailored Laser Surface Patterns on Stainless Steel, *Appl. Surf. Sci.*, 2016, **370**, p 59–66
8. M. Kang, Y.M. Park, B.H. Kim, and Y.H. Seo, Micro- and Nanoscale Surface Texturing Effects on Surface Friction, *Appl. Surf. Sci.*, 2015, **345**, p 344–348
9. C. Lorenzo-Martin and O.O. Ajayi, Effect of Sic Particle Impact Nano-Texturing on Tribological Performance of 304L Stainless Steel, *Appl. Surf. Sci.*, 2014, **315**, p 287–291
10. H.W. Yu, W. Huang, and X.L. Wang, Dimple Patterns Design for Different Circumstances, *Lubr. Sci.*, 2013, **25**, p 67–78
11. Z. Wang, Q. Zhao, C. Wang, and Y. Zhang, Modulation of Dry Tribological Property of Stainless Steel by Femtosecond Laser Surface Texturing, *Appl. Phys. A*, 2015, **119**, p 1155–1163
12. S. Hammouti, B. Beaugiraud, M. Salvia, C. Mauclair, A. Pascale-Hamri, S. Benayoun, and S. Valette, Elaboration of Submicron Structures on PEEK Polymer by Femtosecond Laser, *Appl. Surf. Sci.*, 2015, **327**, p 277–287
13. X.L. Chen, N.S. Qu, H.S. Li, and Z.Y. Xu, Pulsed Electrochemical Micromachining for Generating Micro-Dimple Arrays on a Cylindrical Surface with a Flexible Mask, *Appl. Surf. Sci.*, 2015, **343**, p 141–147
14. R.V. Rao and V.D. Kalyankar, Optimization of Modern Machining Process Using Advanced Optimization Techniques: A Review, *Int. J. Adv. Manuf. Technol.*, 2014, **73**, p 1159–1188
15. Z.Y. Yu, K.P. Rajurkar, and A. Tandon, Study of 3D Micro-Ultrasonic Machining, *J. Manuf. Sci. Eng. Trans. ASME*, 2004, **126**, p 727–732
16. H. Zarepour, S.H. Yeo, P.C. Tan, and E. Aligiri, A New Approach for Force Measurement and Workpiece Clamping in Micro-Ultrasonic Machining, *Int. J. Adv. Manuf. Technol.*, 2011, **53**, p 517–522
17. J.J. Boy, E. Andrey, A. Boulouize, and C. Khan-Malek, Developments in Microultrasonic Machining (MUSM) at FEMTO-ST, *Int. J. Adv. Manuf. Technol.*, 2010, **47**, p 37–45
18. W.L. Zhu, Y.Q. Xing, K.F. Ehmann, and B.F. Ju, Ultrasonic Elliptical Vibration Texturing of the Rake Face of Carbide Cutting Tools for Adhesion Reduction, *Int. J. Adv. Manuf. Technol.*, 2016, **85**, p 2669–2679
19. H.Y. Zhang, Y. Yan, Z.B. Gu, Y. Wang, and T. Sun, Friction Enhancement Between Microscopically Patterned Polydimethylsiloxane and Rabbit Small Intestinal Tract Based on Different Lubrication Mechanisms, *ACS Biomater. Sci. Eng.*, 2016, **2**, p 900–907
20. Q.F. Wang, Y.X. Wang, H.L. Wang, N. Fan, and F.Y. Yan, Experimental Investigation on Tribological Behavior of Several Polymer Materials Under Reciprocating Sliding and Fretting Wear Conditions, *Tribol. Int.*, 2016, **104**, p 73–82